Soliton excitations in halogen-bridged mixed-valence binuclear metal complexes

Shoji Yamamoto and Masanori Ichioka
Department of Physics, Okayama University, Tsushima, Okayama 700-8530, Japan
(Received 15 August 2001)

Motivated by recent stimulative observations in halogen (X)-bridged binuclear transition-metal (M) complexes, which are referred to as MMX chains, we study solitons in a one-dimensional three-quarter-filled charge-density-wave system with both intrasite and intersite electron-lattice couplings. Two distinct ground states of MMX chains are reproduced and the soliton excitations on them are compared. In the weak-coupling region, all the solitons are degenerate to each other and are uniquely scaled by the band gap, whereas in the strong-coupling region, they behave differently deviating from the scenario in the continuum limit. The soliton masses are calculated and compared with those for conventional mononuclear MX chains.

PACS numbers: 71.10.Hf, 71.45.Lr, 71.38.+i

I. INTRODUCTION

Quasi-one-dimensional halogen (X)-bridged transition-metal (M) complexes [1], which are referred to as MX chains, have been attracting much interest because of their unique behavior featured by electron-electron correlations, electron-lattice interactions, low dimensionality and *d*-*p* orbital hybridization [2,3]. The PtX compounds [4–6] have mixed-valence ground states exhibiting intense and dichroic charge-transfer absorption, strong resonance enhancement of Raman spectra and luminescence with large Stokes shift. On the other hand, the NiX compounds [7–9] possess monovalence magnetic ground states due to the strong on-site *d*-*d* Coulomb interaction. Substituting the bridging halogens, ligand molecules and counter ions as well as the transition metals, we can widely tune the electronic states of MX chains [10].

Solitonic excitations inherent in doubly degenerate charge-density-wave systems stimulate further interest in MX materials. In this context, we may first be reminded of polyacetylene, the trans isomer of which exhibits topological solitons, or moving domain walls. Electron-spin-resonance measurements [11,12] on trans-polyacetylenes demonstrated the existence of highly mobile neutral magnetic defects, while infrared absorption spectra [13] for lightly doped ones illuminated the formation of charged domain walls. Such observations were finely interpreted employing a simple but relevant model Hamiltonian [14–16]. The soliton picture established for polyacetylene led to an idea [17,18] of similar defect states existing in MX chains. Although MX chains could not electrochemically be doped, photogenerated solitons were extensively observed [19,20] in PtX chains.

In recent years, a new class of halogen-bridged metal complexes, which consist of alternating binuclear metal complexes and halogen ions and are thus referred to as MMX chains, have renewed our interest in this system. In comparison with MX chains, MMX chains indeed look more interesting. The formal oxidation state of the metal ions is 3+ in MX chains, whereas it is 2.5+ in MMX chains. Therefore, MMX chains have an unpaired electron per metal dimer even in their trapped-valence states, contrasting with the valence-trapped state consisting of M^{2+} and M^{4+} in MX chains. The M(d_{z^2})-M(d_{z^2}) direct overlap in MMX chains effectively reduces the on-site Coulomb repulsion due to its d_{σ^*} character and therefore enhances the electrical conductivity.

The actual observations of MMX chains are really stimulative. The thus-far synthesized MMX compounds comprise two families: $M_2(dta)_4I$ (M = Pt, Ni; dta = dithioacetate = $CH_3CS_2^-$) [21,22] and $R_4[Pt_2(pop)_4X]\cdot nH_2O$ (X = Cl, Br, I; R = Li, K, Cs, $\cdots$; pop = diphosphonate = $P_2O_5H_2^{2-}$) [23,24]. The former, dta complexes, are not yet well investigated but one of them, $Pt_2(dta)_4I$, has now come into hot argument due to its fascinating features [25]. $Pt_2(dta)_4I$ exhibits metallic conduction around room temperature, which is the first observation in one-dimensional halogen-bridged metal complexes. With decreasing temperature, there occurs a metal-semiconductor transition at 300 K and further transition to the Peierls-insulating charge-ordering mode, which is shown in Fig. 1(b), follows around 80 K. The alternate-charge-polarization (ACP) state is accompanied by metal-sublattice dimerization, which has never been observed in MX compounds. $Pt_2(dta)_4I$ has a neutral chain structure, where the metal sublattice gets rid of any hydrogen-bond network and therefore exhibits more pronounced one dimensionality. The novel two-step thermal behavior has recently been supported theoretically [26]. On the other hand, the latter, pop complexes, have extensively been measured [24,27–30] and their ground states have in general been assigned to charge-density-wave (CDW) states of the conventional type, which are shown in Fig. 1(a). However, a large choice of bridging halogens, ligand molecules and counter ions in the pop complexes results in a wide tunability of their ground states [31]. Such a tuning of the electronic state can be realized also by pressure [32–34]. It is interesting that an applied pressure diminishes the Peierls gap at low temperatures [35,36] but oppositely stabilizes the CDW state at higher temperatures [37].

Local states of MMX chains, whether photogenerated

or doping-induced ones, must be a coming potential subject. The photoinduced-absorption spectrum has just been measured to reveal the intrinsic charge-transfer excitations, but the photoexperiments [38] are still in their early stage. Though the optical conductivity has recently been calculated [39], any microscopic information on the defect states remains lacking. In such circumstances, we give a detailed report on soliton excitations in MMX chains making full use of electron-phonon models. Such an approach as regards electron-lattice interactions as most important not only successfully interpreted the excitation spectrum of polyacetylene [14–16,41–44] but also clarified characteristic excitations [18,36] of MX chains. The analytic aspect [16,18] of the class of electron-phonon models further stimulates our interest. Since recent extensive calculations [26,40] of the MMX system have shown that the dta and pop complexes are mainly characterized by their distinct electron-lattice interactions, our starting point is well justified from the practical point of view as well. Let us take the first step toward explorations into nonlinear excitations in mixed-valence binuclear metal complexes.

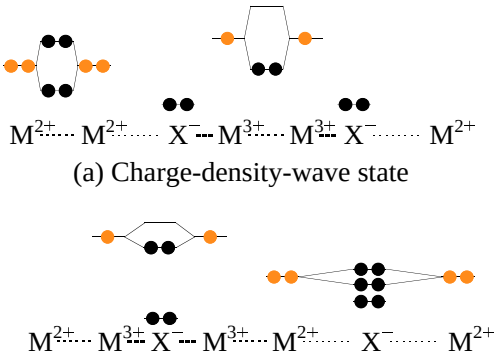

FIG. 1. Schematic representation of the two distinct ground states of MMX chains: (a) Charge-density-wave (CDW) state whose X sublattice is dimerized; (b) Alternate charge-polarization (ACP) state whose M_2 sublattice is dimerized.

II. GROUND-STATE PROPERTIES

We introduce the $\frac{3}{4}$-filled one-dimensional single-band two-orbital electron-phonon model:

$$\begin{aligned}\mathcal{H} = & -t_{\rm MM}\sum_{n,s}(a^\dagger_{n,s}b_{n,s}+b^\dagger_{n,s}a_{n,s}) \\ & -\sum_{n,s}\left[t_{\rm MXM}-\alpha(v_{n+1}-v_n)\right](b^\dagger_{n,s}a_{n+1,s}+a^\dagger_{n+1,s}b_{n,s}) \\ & -\beta\sum_{n,s}\left[(v_n-u_{n-1})a^\dagger_{n,s}a_{n,s}+(u_n-v_n)b^\dagger_{n,s}b_{n,s}\right] \\ & +\frac{K_{\rm MX}}{2}\sum_n\left[(u_n-v_n)^2+(v_n-u_{n-1})^2\right], \qquad (2.1)\end{aligned}$$

where $a^\dagger_{n,s}$ and $b^\dagger_{n,s}$ are the creation operators of an electron with spin $s=\pm$ (up and down) for the M d_{z^2} orbitals in the nth MMX unit, which we refer to as a- and b-metal sites. $t_{\rm MM}$ and $t_{\rm MXM}$ describe the electron hoppings between neighboring metal sites. α and β are the intersite and intrasite electron-phonon coupling constants, respectively, with $K_{\rm MX}$ being the metal-halogen spring constant. u_n and v_n are, respectively, the chain-direction displacements of the halogen and metal dimer in the nth MMX unit from their equilibrium position. We assume, based on the thus-far reported experimental observations, that every M_2 moiety is not deformed. We set $t_{\rm MM}$ and K both equal to unity unless a particular mention.

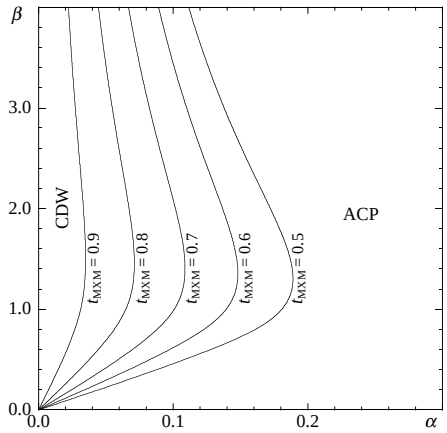

FIG. 2. The α-versus-β ground-state phase diagram as a function of $t_{\rm MXM}$.

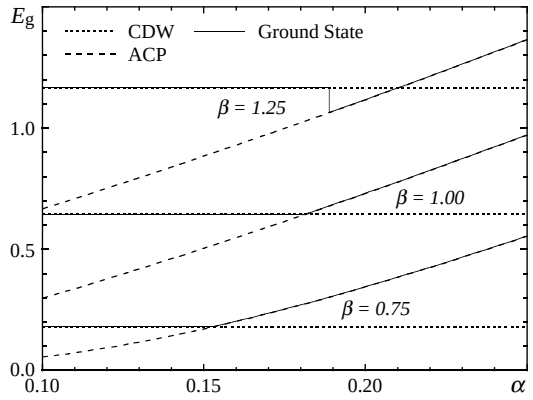

FIG. 3. The competing Peierls gaps of the CDW and ACP states and the consequent band gap as functions of α and β.

This Hamiltonian possesses two distinct ground states which are shown in Fig. 1 and their competition is visualized in Fig. 2. The CDW state is characterized by the alternating on-site energies, whereas the ACP state comparatively by the alternating interdimer transfer energies. The orbital hybridization within every M_2 moiety is essential in the valence-trapped CDW state, while it is the overlap of the d_{σ^*} orbitals on neighboring M_2 moieties that stabilizes the valence-delocalized ACP state.

Therefore, increasing β and $t_{\rm MM}$ advantageously act on the CDW state, whereas increasing α and $t_{\rm MXM}$ on the ACP state. When $t_{\rm MM} = t_{\rm MXM}$ and $\alpha = 0$, the CDW and ACP states are degenerate to each other regardless of β.

The phase transition between the two states is of the first order. We plot in Fig. 3 the Peierls gaps as functions of the coupling constants. The band gap varies continuously across the phase boundary in the weak-coupling region, whereas it exhibits a discontinuity in the strong-coupling region. The ACP state depends on both α and β, but the CDW state has no dependence on α. The intersite electron-phonon coupling originates in distortion of the M_2 sublattice.

The calculations are well consistent with the experimental observations; the pop-family compounds $(NH_4)_4[Pt_2(pop)_4X]$ exhibit ground states of the CDW type [29], while the dta complex $Pt_2(dta)_4I$ displays that of the ACP type [25]. The M_2 moieties are tightly locked together in the pop complexes due to the hydrogen bonds between the ligands and the counter cations, whereas they are much more movable in $Pt_2(dta)_4I$ owing to its neutral chain structure. Thus, considering that α indirectly describes the mobility of the M_2 sublattice, a significantly larger α is expected for $Pt_2(dta)_4I$.

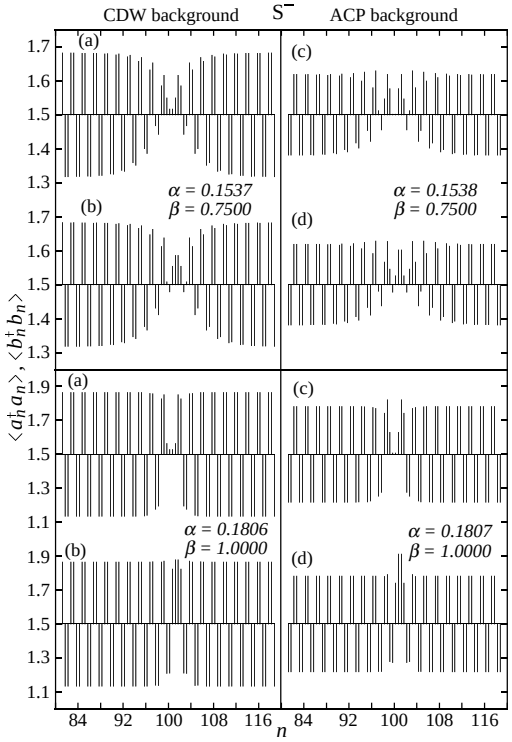

FIG. 4. Electronic structures of the negatively charged solitons in the CDW (a and b) and ACP (c and d) states, where quantum averages of the local electron densities are measured in comparison with the average occupancy: (a) $x_0 = 100.5$ with the highest energy; (b) $x_0 = 101.5$ with the lowest energy; (c) $x_0 = 100$ with the highest energy; (d) $x_0 = 101$ with the lowest energy.

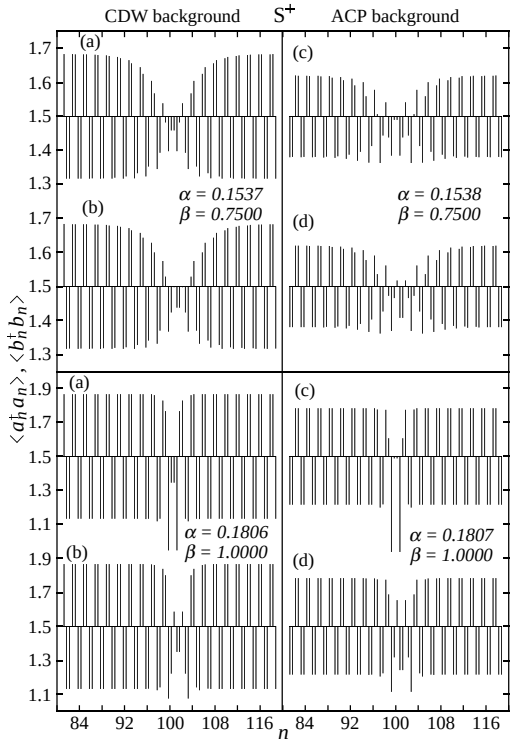

FIG. 5. The same as Fig. 4 but the positively charged solitons: (a) $x_0 = 100.5$ with the lowest energy; (b) $x_0 = 101.5$ with the highest energy; (c) $x_0 = 100$ with the lowest energy; (d) $x_0 = 101$ with the highest energy.

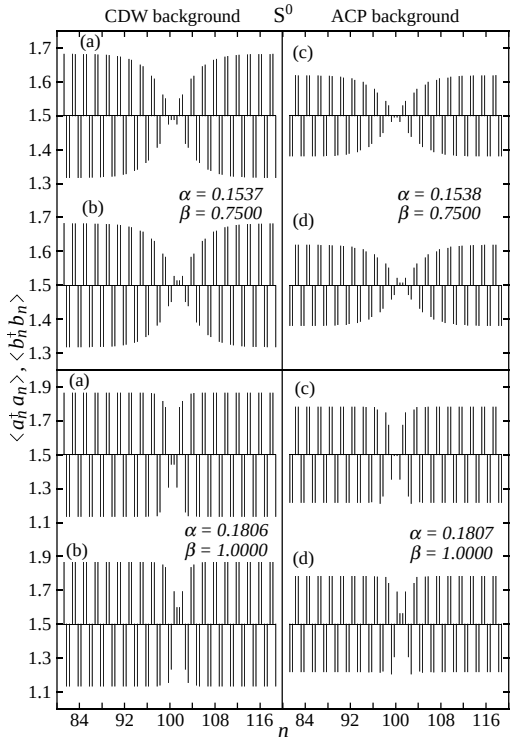

FIG. 6. The same as Fig. 4 but the neutral solitons: (a) $x_0 = 100.5$ with the highest energy; (b) $x_0 = 101.5$ with the lowest energy; (c) $x_0 = 100$ with the highest energy; (d) $x_0 = 101$ with the lowest energy.

III. SOLITON EXCITATIONS

Now we search for soliton solutions of the Hamiltonian (2.1). Under the constraint of the total chain length being unchanged, a trial wave function may be introduced as [14,15]

$$u_n - v_n = \sigma(v_{n+1} - u_n) = (-1)^n l_0 \tanh\bigl[(na - x_0)/\xi_{\rm s}\bigr]\,, \tag{3.1}$$

where σ takes $-$ and $+$ for the CDW and ACP backgrounds, respectively, a is the lattice constant (the original unit-cell length), l_0 is the metal-halogen bond-length change in the ground state, and x_0 and $\xi_{\rm s}$ are, respectively, the soliton center and width, both of which are variationally determined. Since we impose the periodic boundary condition on the Hamiltonian, the soliton solutions demand that the number of the original unit cells, N, should be odd. We set N equal to 201, which is much larger than $\xi_{\rm s}$ in any calculation of ours. Then, negatively-charged ($\rm S^-$), positively-charged ($\rm S^+$) and neutral ($\rm S^0$) solitons are obtained by setting $N_+ = N_- = 302$, $N_+ = N_- = 301$ and $N_\pm = N_\mp + 1 = 302$, respectively, where N_s is the number of the electrons with spin s. Due to the spin-rotational symmetry, the neutral solitons with up and down spins are degenerate to each other. The degeneracy between the neutral and charged solitons may be lifted in the strong-coupling region. When we compare the solitons with the CDW and ACP backgrounds, we calculate them in the vicinity of the phase boundary so as to illuminate their essential differences, if any. Taking the structural analyses [21,23,24] into consideration, we set $t_{\rm MM} = 2t_{\rm MXM}$.

A. Wave Functions

We show the spatial configurations of $\rm S^-$, $\rm S^+$ and $\rm S^0$ in Figs. 4, 5 and 6, respectively. Their formation energies $E_{\rm s}$ do not depend on their locations in the weak-coupling region, but the degeneracy is lifted in the strong-coupling region. Two of the differently-located solitons are shown at each parametrization, one of which has the highest energy as a function of x_0, while the other of which is the optimum configuration. As the coupling strength increases, solitons generally possess increasing energies and end up with immobile defects.

$\xi_{\rm s}$ looks like a decreasing function of α and β. In order to illuminate its scaling behavior in more detail, we plot in Fig. 7 $\xi_{\rm s}$ as a function of the band gap $E_{\rm g}$. Although we take α and β at random, $\xi_{\rm s}$ is uniquely scaled by $E_{\rm g}$ as far as $E_{\rm g}$ stays not so large. We obtain a scaling formula

$$\xi_{\rm s}/a \simeq 0.96/E_{\rm g}^{0.98}\,, \tag{3.2}$$

though there is large uncertainty in the second decimal place according to data set adopted into the fitting. The scaling relation fits all the solitons $\rm S^\pm$ and $\rm S^0$. It is quite convincing that such a scaling law breaks down as $\xi_{\rm s}$ approaches a, where the chain no more behaves as a continuum. We return to Eq. (3.2) later in an argument in the continuum limit.

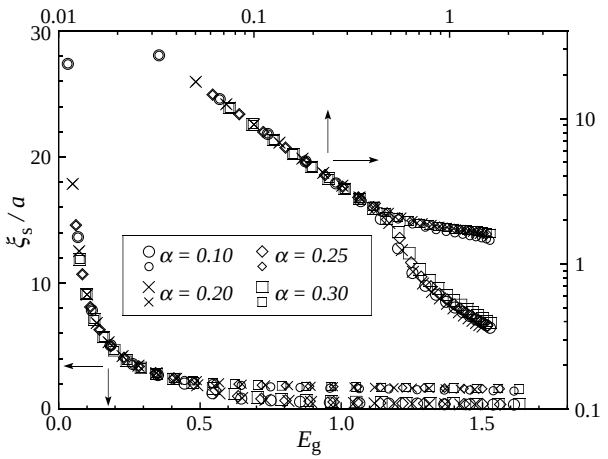

FIG. 7. The optimized width of the negatively charged soliton as a function of the band gap $E_{\rm g}$ in linear and logarithmic scales under various parametrizations, where the larger and smaller symbols correspond to the lowest- and highest-energy locations x_0, respectively.

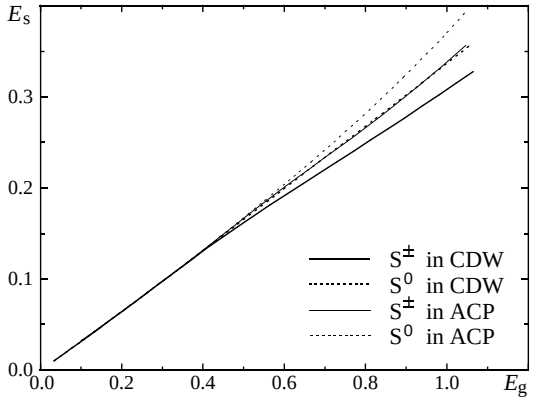

FIG. 8. The soliton formation energies $E_{\rm s}$ as functions of the band gap $E_{\rm g}$, where $E_{\rm s}$ is averaged over x_0. The negatively and positively charged solitons possess more and less than three-quarter-filled electron bands, respectively, and therefore their formation energies can not be defined in themselves. As for the charged solitons, $E_{\rm s}$ is further averaged over $\rm S^+$ and $\rm S^-$.

The degeneracy with respect to the soliton type and location is lifted in the strong-coupling region where $\xi_{\rm s} \lesssim a$. In Fig. 8 we plot $E_{\rm s}$ as a function of $E_{\rm g}$ for various soliton solutions. As the band gap grows, $\rm S^0$ generally comes to have a higher energy than $\rm S^\pm$, which is the case in MX chains as well. The simplest argument in the strong-coupling region may be the atomic treatment of electrons. Setting $t_{\rm MXM} = 0$ in an MX chain with the CDW ground state, we obtain the soliton energies as $E_{\rm s}(\rm S^0) = 3E_{\rm g}/4$

and $E_{\rm s}(\mathrm{S}^{\pm}) = E_{\rm g}/2$ [36], where $2E_{\rm g} \equiv 4\beta^2/K$ is the Peierls gap in the atomic limit. A similar argument in the present case is not so trivial. The CDW and ACP states are stabilized by sufficient M-M intradimer and M-X-M interdimer electronic communications, respectively (see Fig. 1). Therefore, even in the strong-coupling region, we can not reasonably set $t_{\rm MM} = t_{\rm MXM} = 0$ but should treat the hybridized d_{σ^*} orbitals under the situations, $t_{\rm MXM} \ll t_{\rm MM} \lesssim \beta$ and $t_{\rm MM} \ll t_{\rm MXM} \lesssim \beta$, for the CDW and ACP backgrounds, respectively. Such calculations still imply that $E_{\rm s}(\mathrm{S}^{\pm}) < E_{\rm s}(\mathrm{S}^0)$.

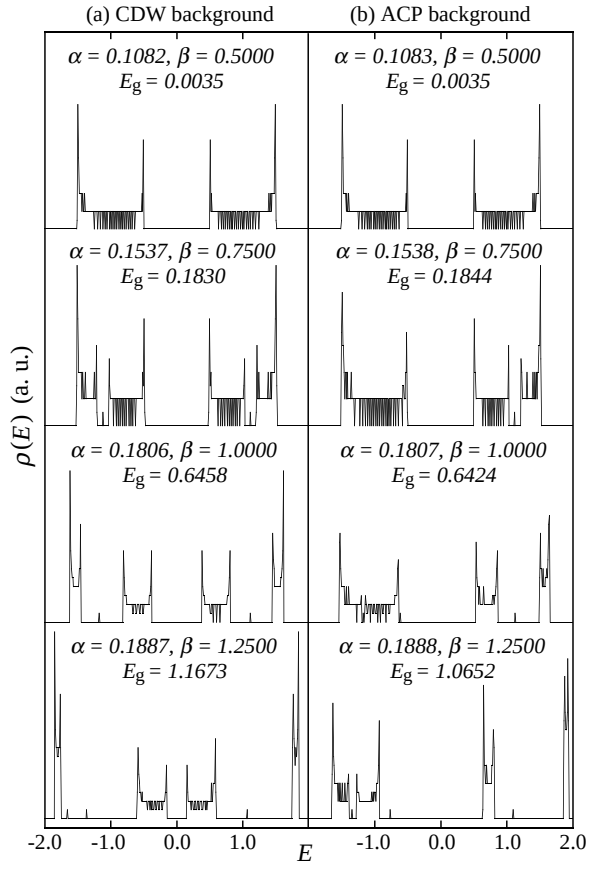

FIG. 9. Density of states $\rho(E)$ for the optimum soliton solutions with the CDW (a) and ACP (b) backgrounds.

B. Energy Structures

Density of states for the optimum soliton solutions are shown in Fig. 9. The background spectrum generally consists of four bands due to the ground-state cell doubling. The four bands of the CDW state are, from the bottom to the top, largely made up of the bonding combination ϕ_+ of binuclear Pt^{2+}-Pt^{2+} units, that of Pt^{3+}-Pt^{3+} units, the antibonding combination ϕ_- of Pt^{2+}-Pt^{2+} units and that of Pt^{3+}-Pt^{3+} units. On the other hand, the major components of the four bands of the ACP state are the ϕ_+ orbitals of interdimer Pt^{2+}-X^{-}-Pt^{2+} units, the ϕ_- orbitals of Pt^{2+}-X^{-}-Pt^{2+} units, the ϕ_+ orbitals of Pt^{3+}-X^{-}-Pt^{3+} units and the ϕ_- orbitals of Pt^{3+}-X^{-}-Pt^{3+} units. Thus, increasing β splits both σ and σ^* orbitals in the CDW state but comparatively enhances the splitting between σ and σ^* orbitals in the ACP state.

The optimum soliton solutions commonly exhibit an additional level within the gap. In contrast with the case of polyacetylene [14,15], the soliton levels generally deviate from the middle of the gap in MMX chains as a result of the breakdown of the electron-hole symmetry. Besides the intragap level, there appear a few related levels depending upon the coupling strength. As far as we work with electron-phonon Hamiltonians without any Coulomb interactions, the level structure does not vary with the soliton charge.

Figure 10 shows local density of states for the optimum soliton solutions. Solitons are indeed localized around their centers. The probability density of the solitons generally oscillates according as n is even or odd, which is the same observations that we find in the Su-Schrieffer-Heeger (SSH) model [14,15] of polyacetylene. The oscillation is more remarkable on the ACP background, which is convincing when we compare the binuclear metal units to the CH groups in polyacetylene. However, the ACP solitons in MMX chains have little probability at their centers in contrast with the SSH solitons exhibiting the largest probability at their centers. Their opposite oscillating behaviors may be ascribed to their distinct electron-phonon interactions of the Holstein (intrasite) and SSH (intersite) type.

IV. DISCUSSION

A. The Continuum Limit

The discovery of a rigorous soliton solution in the Takayama-Lin-Liu-Maki (TLM) model [16], which is the continuum version of the SSH model for polyacetylene, significantly stimulated the theoretical investigations of MX chains. On the analogy of the twofold degeneracy of the ground state, Ichinose [17] proposed an idea of topological solitons governing the lattice relaxation of charge-transfer excitations in mixed-valence MX chains. Onodera [18] further demonstrated that solitons should play an important role in MX chains as well, pointing out the equivalence of an MX chain to a CH chain in the continuum limit. Since then nonlinear excitations in MX chains have also extensively been calculated [2,3,35,36,45–52] and indeed been observed experimentally [19,20,53–55].

Figure 7 has revealed that there still holds a scaling law for soliton excitations in the MMX system. In the weak-coupling region, the soliton width is uniquely scaled by the band gap regardless of the ground-state properties. The TLM model powerfully illuminated the scaling properties of CH chains and was successfully tuned so as to describe MX chains. Here we consider the continuum description of MMX chains.

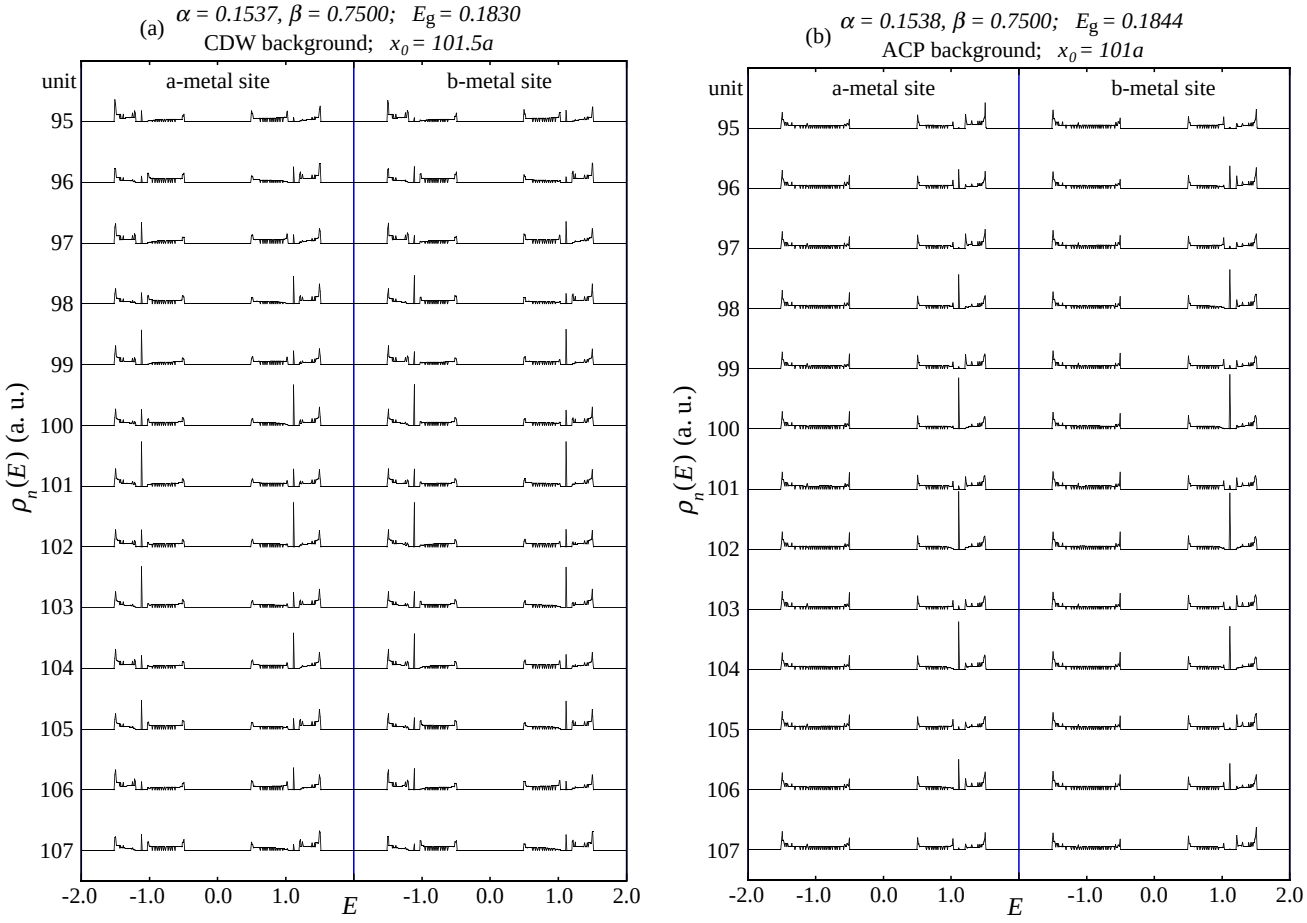

FIG. 10. Local density of states $\rho_n(E)$ for the optimum soliton solutions with the CDW (a) and ACP (b) backgrounds.

In order to derive the continuum version of the present model (2.1), it is essential to describe an MMX chain in terms of effectively half-filled electron bands. Therefore, we first neglect the electron-phonon coupling in the Hamiltonian (2.1) and obtain

$$\lim_{\alpha,\beta\to 0}\mathcal{H}=\sum_{k,s}\left(\varepsilon_k^+A_{k,s}^\dagger A_{k,s}+\varepsilon_k^-B_{k,s}^\dagger B_{k,s}\right)\,, \tag{4.1}$$

where

$$\varepsilon_k^\pm=\pm\sqrt{t_{\rm MM}^2+t_{\rm MXM}^2+2t_{\rm MM}t_{\rm MXM}\cos ka}\,, \tag{4.2}$$

$$\begin{aligned} A_{k,s} &= \frac{1}{\sqrt{2}}\left(\mathrm{e}^{\mathrm{i}\theta/2}a_{k,s}+\mathrm{e}^{-\mathrm{i}\theta/2}b_{k,s}\right)\,,\\ B_{k,s} &= \frac{1}{\sqrt{2}}\left(\mathrm{e}^{\mathrm{i}\theta/2}a_{k,s}-\mathrm{e}^{-\mathrm{i}\theta/2}b_{k,s}\right)\,, \end{aligned} \tag{4.3}$$

with

$$\mathrm{e}^{\mathrm{i}\theta}=-\frac{t_{\rm MM}+t_{\rm MXM}\mathrm{e}^{\mathrm{i}ka}}{\sqrt{t_{\rm MM}^2+t_{\rm MXM}^2+2t_{\rm MM}t_{\rm MXM}\cos ka}}\,, \tag{4.4}$$

$$\begin{aligned} a_{k,s} &= \frac{1}{\sqrt{N}}\sum_{k,s}\mathrm{e}^{-\mathrm{i}kna}a_{n,s}\,,\\ b_{k,s} &= \frac{1}{\sqrt{N}}\sum_{k,s}\mathrm{e}^{-\mathrm{i}kna}b_{n,s}\,. \end{aligned} \tag{4.5}$$

Since we are interested in the low-lying excitations governed by the electronic structure near the Fermi level, we discard the irrelevant band ε_k^- and linearize the relevant dispersion relation ε_k^+ at the two Fermi points. Then, assuming the CDW and ACP ground states, we reach effective Hamiltonians in the coordinate representation:

$$\begin{aligned} \mathcal{H}_{\rm eff}^{\rm CDW} &= t_{\rm eff}\sum_{n,s}\left[1-\frac{\Delta(na)}{t_{\rm MM}}\right]\left(A_{n,s}^\dagger A_{n+1,s}+\mathrm{H.c.}\right)\\ &+\frac{2t_{\rm eff}}{t_{\rm MXM}}\sum_{n,s}\Delta(na)A_{n,s}^\dagger A_{n,s}+\frac{K_{\rm MX}}{4\beta_{\rm eff}^2}\sum_n\Delta(na)^2\,, \end{aligned} \tag{4.6}$$

$$\begin{aligned} \mathcal{H}_{\rm eff}^{\rm ACP} &= t_{\rm eff}\sum_{n,s}\left[1-\frac{\Delta(na)}{t_{\rm MXM}}\right]\left(A_{n,s}^\dagger A_{n+1,s}+\mathrm{H.c.}\right)\\ &+\frac{2t_{\rm eff}}{t_{\rm MM}}\sum_{n,s}\Delta(na)A_{n,s}^\dagger A_{n,s}+\frac{K_{\rm MX}}{16\alpha_{\rm eff}^2}\sum_n\Delta(na)^2\,, \end{aligned} \tag{4.7}$$

where

$$t_{\rm eff}=\frac{t_{\rm MM}t_{\rm MXM}}{2\sqrt{t_{\rm MM}^2+t_{\rm MXM}^2}}\,, \tag{4.8}$$

$$\alpha_{\rm eff} = \frac{1}{2}\left(\alpha + \frac{t_{\rm eff}}{t_{\rm MM}}\beta\right)\ , \quad \beta_{\rm eff} = \frac{t_{\rm eff}}{t_{\rm MXM}}\,, \tag{4.9}$$

$$\Delta(na) = \begin{cases} 2\beta_{\rm eff}(-1)^n(u_n - v_n) & \text{for } \mathcal{H}_{\rm eff}^{\rm CDW}\,, \\ 4\alpha_{\rm eff}(-1)^n(u_n - v_n) & \text{for } \mathcal{H}_{\rm eff}^{\rm ACP}\,. \end{cases} \tag{4.10}$$

The gap parameter $\Delta(na)$ is constant in the ground state and is expected to show smooth and slow spatial variations for the relevant fluctuations. Correspondingly we introduce slowly-varying field operators

$$\begin{aligned} \psi_s^{(r)}(na) &= \frac{1}{\sqrt{L}}\sum_k {\rm e}^{{\rm i}kna} A_{k_{\rm F}+k,s}\,, \\ \psi_s^{(l)}(na) &= \frac{-{\rm i}}{\sqrt{L}}\sum_k {\rm e}^{{\rm i}kna} A_{-k_{\rm F}+k,s}\,, \end{aligned} \tag{4.11}$$

for right- and left-moving electrons, respectively, where $L = Na$, $k_{\rm F} = \pi/2a$ and $-\pi/2a < k \le \pi/2a$. Now, summing out fast-varying components and taking the continuum limit $a \to 0$, the lattice description can be mapped onto a continuous line as

$$\begin{aligned} \mathcal{H}_{\rm eff}^{\rm CDW} = \int \frac{\Delta(x)^2}{2\pi\hbar v_{\rm F}\lambda}{\rm d}x + \sum_s \int \Phi_s^\dagger(x)\Bigg[{\rm i}\hbar v_{\rm F}\sigma_z\frac{\rm d}{{\rm d}x} \\ -2\Delta(x)t_{\rm eff}\left(\frac{\sigma_x}{t_{\rm MM}} + \frac{\sigma_y}{t_{\rm MXM}}\right)\Bigg]\Phi_s(x){\rm d}x\,, \end{aligned} \tag{4.12}$$

$$\begin{aligned} \mathcal{H}_{\rm eff}^{\rm ACP} = \int \frac{\Delta(x)^2}{2\pi\hbar v_{\rm F}\lambda}{\rm d}x + \sum_s \int \Phi_s^\dagger(x)\Bigg[{\rm i}\hbar v_{\rm F}\sigma_z\frac{\rm d}{{\rm d}x} \\ -2\Delta(x)t_{\rm eff}\left(\frac{\sigma_x}{t_{\rm MXM}} + \frac{\sigma_y}{t_{\rm MM}}\right)\Bigg]\Phi_s(x){\rm d}x\,, \end{aligned} \tag{4.13}$$

with the Pauli matrices $(\sigma_x, \sigma_y, \sigma_z)$ and a spinor notation $\Phi_s^\dagger(x) = (\psi_s^{(r)}(x)^*, \psi_s^{(l)}(x)^*)$. Here the Fermi velocity $v_{\rm F}$ and the dimensionless coupling constant λ has, respectively, been defined as

$$\hbar v_{\rm F} = 2at_{\rm eff}\,, \tag{4.14}$$

$$\lambda = \begin{cases} \beta_{\rm eff}^2/\pi t_{\rm eff}K_{\rm MX} & \text{for } \mathcal{H}_{\rm eff}^{\rm CDW}, \\ 4\alpha_{\rm eff}^2/\pi t_{\rm eff}K_{\rm MX} & \text{for } \mathcal{H}_{\rm eff}^{\rm ACP}. \end{cases} \tag{4.15}$$

Interestingly, both Hamiltonians (4.12) and (4.13) are mathematically equivalent to the TLM model

$$\begin{aligned} \mathcal{H}_{\rm TLM} = \int \frac{\Delta(x)^2}{2\pi\hbar v_{\rm F}\lambda}{\rm d}x + \sum_s \int \Phi_s^\dagger(x) \\ \times\left[-{\rm i}\hbar v_{\rm F}\sigma_z\frac{\rm d}{{\rm d}x} + \Delta(x)\sigma_x\right]\Phi_s(x){\rm d}x\,, \end{aligned} \tag{4.16}$$

because they can exactly be transformed into Eq. (4.16), except for the minus sign attached to the σ_z term, by rotating the spinor wave function around the z axis as $\exp({\rm i}\varphi\sigma_z/2)\Phi_s(x)$ with $\tan\varphi$ being equal to $t_{\rm MM}/t_{\rm MXM}$ and $t_{\rm MXM}/t_{\rm MM}$ for $\mathcal{H}_{\rm eff}^{\rm CDW}$ and $\mathcal{H}_{\rm eff}^{\rm ACP}$, respectively. The Hamiltonian (4.16) possesses, regardless of the sign of its σ_z term, an exact solution of the form (3.1) [16,41]. Consequently the equivalent Hamiltonians (4.12) and (4.13) also give the soliton solution

$$\Delta(x) = \Delta_0 \tanh\left[(x - x_0)/\xi_{\rm s}\right]\,, \tag{4.17}$$

with the TLM scaling relation and formation energy

$$\xi_{\rm s} = \hbar v_{\rm F}/\Delta_0 = 4at_{\rm eff}/E_{\rm g}\,, \tag{4.18}$$

$$E_{\rm s} = 2\Delta_0/\pi = E_{\rm g}/\pi\,. \tag{4.19}$$

When we substitute the condition $t_{\rm MM} = 2t_{\rm MXM}$ into Eq. (4.18), we obtain $\xi_{\rm s} = 2a/\sqrt{5}E_{\rm g}$, which explains well the numerical findings (3.2). Figure 8 demonstrates the unique behavior of the solitons in the weak-coupling region claiming that

$$E_{\rm s} \simeq 0.32E_{\rm g}\,, \tag{4.20}$$

which is also in good agreement with Eq. (4.19).

B. The Effective Mass

The soliton mass $M_{\rm s}$ can be calculated by considering a slowly-moving domain wall, that is, substituting $x_0 = v_{\rm s}t$ into Eq. (3.1). Neglecting any change in the wall shape, which must be of order $v_{\rm s}^2$, we obtain

$$\frac{1}{2}M_{\rm s}v_{\rm s}^2 = \frac{1}{2}M\sum_n\left[\frac{\rm d}{{\rm d}t}(u_n - v_n)\right]^2 = \frac{2Ml_0^2v_{\rm s}^2}{3a\xi}\,, \tag{4.21}$$

within the adiabatic approximation, where M corresponds to the halogen mass for $R_4[Pt_2(pop)_4X]\cdot nH_2O$ with the CDW ground state and to the mass of the binuclear platinum complex $Pt_2(dta)_4$ for $Pt_2(dta)_4I$ with the ACP ground state.

Since there is little information available on electronic parameters such as hopping amplitudes in MMX chains, we continue to work with the condition $t_{\rm MM} = 2t_{\rm MXM}$. Among plenty of adjustable parameters, we lay great importance on the band gap $E_{\rm g}$, which can reliably be measured in general. We first discuss the pop complexes, which are similar to MX chains in structure and therefore allow us to rely upon a good knowledge of the MX system. There is increased distortion of the halogen sublattice in the order I < Br < Cl [28], in which the halogen mass oppositely decreases. Considering their contributions to the soliton mass, $M_{\rm s} \propto Ml_0^2$, solitons turn out most mobile in the iodo complexes [18]. The smaller gap, the larger mobility of solitons. Hence we take a sample material $Na_4[Pt_2(pop)_4I]\cdot 7H_2O$ [38] with the CDW ground state of $E_{\rm g} = 1.2\,{\rm eV}$. Its structural data are available as $a = 8.9\,$Å and $l_0 = 0.3\,$Å. For lack of a few more parameters, we depend on calculations of PtI compounds. Baeriswyl and Bishop (BB) [35] estimate that $t_{\rm MXM} = 0.8\,{\rm eV}$ and $K_{\rm MX} = 8.9\,{\rm eV\AA}^{-2}$, while Tagawa

and Suzuki (TS) [52] claim that $t_{\rm MXM} = 1.52\,{\rm eV}$ and $K_{\rm MX} = 11.47\,{\rm eV\AA}^{-2}$. Standing on the experimental findings $E_{\rm g} = 1.2\,{\rm eV}$ and $a = 8.9\,\text{Å}$ with the help of the BB and TS parametrizations, the lattice distortion l_0 turns out 0.18 Å and 0.13 Å, respectively, the former of which is closer to the observations. The resultant soliton features are summarized in Table I, where $m_{\rm e}$ is the free-electron mass. In any case the estimated mass is smaller than that for PtI chains, $M_{\rm s} \sim 200 m_{\rm e}$ [18]. Polynuclear metal units contribute toward suppressing l_0 and enlarging a and thus end up with smaller soliton masses. However, the soliton masses in the pop complexes still stay much larger than those in polyacetylene, $M_{\rm s} \sim 6 m_{\rm e}$ [14,15]. This is because most of the existent pop-family compounds lie in a rather strong-coupling region. Recently there has appeared an interesting attempt [31] to tune the Peierls gap of the pop complexes by replacing their counter ions. Such explorations may further enhance the soliton mobility.

Another possibility may lie in the dta complex. $Pt_2(dta)_4I$ exhibits a smaller gap [25] probably due to its smaller $Pt-Pt$ distance [21] and increased mixing of halide character in the d_σ $Pt-Pt$ wave function [40]. The crystalline structure of $Pt_2(dta)_4I$ is much different from those of MX chains and therefore we do not have any useful information on its electronic parameters. Relying upon the experimental findings, $E_{\rm g} = 0.3\,{\rm eV}$ [25] and $a = 8.6\,\text{Å}$ [21], and assuming that $t_{\rm MM} = 2t_{\rm MXM} = 2\,{\rm eV}$ and 1.5 eV together with $K_{\rm MX} = 8.9\,{\rm eV\AA}^{-2}$, we give trial estimates in Table II. Considering the smaller $Pt-Pt$ distance, the results with $t_{\rm MM} = 1.5\,{\rm eV}$ may be too conservative. Anyway $Pt_2(dta)_4I$ is likely to have much more mobile solitons than the pop complexes.

Metal polynucleation leads to a smaller gap and thus suppresses the soliton mass. This must be the case with the pop complexes, more generally, with the family compounds exhibiting the ground states of the CDW type. However, it may not necessarily be the case with the dta complex, that is, with the family compounds which possess neutral chain structures and therefore exhibit the ACP-type ground states, where increasing M may prevent $M_{\rm s}$ from decreasing. The usual metallic conduction, rather than a solitonic one, may be much more relevant in such polynuclear metal complexes.

V. SUMMARY

We have demonstrated the soliton excitations in MMX chains laying emphasis on both similarities and differences between the cases of the CDW and ACP backgrounds. Solitons in the weak-coupling region are all degenerate to each other and are uniquely scaled by the band gap, whether it originates in the CDW or ACP instability. The degeneracy is lifted in the strong-coupling region, where neutral solitons come to have higher energies than charged solitons. Solitons are likely to be more mobile in MMX chains than in MX chains. We are hoping for a systematic observation on various binuclear and possibly polynuclear [56] metal complexes.

ACKNOWLEDGMENTS

The authors are grateful to Prof. K. Yonemitsu for fruitful discussion. They further thank Prof. H. Okamoto for helpful information on MMX materials. This work was supported by the Japanese Ministry of Education, Science, Sports and Culture. The numerical calculation was done using the facility of the Supercomputer Center, Institute for Solid State Physics, University of Tokyo.

[1] R. J. H. Clark: *Advances in Infrared and Raman Spectroscopy*, ed. R. J. H. Clark and R. E. Hester (Wiley, New York, 1984) Vol. II, p. 95.
[2] J. T. Gammel, A. Saxena, I. Batistić, A. R. Bishop and S. R. Phillpot: Phys. Rev. B **45** (1992) 6408.
[3] S. W. Weber-Milbrodt, J. T. Gammel, A. R. Bishop, and E. Y. Loh, Jr., Phys. Rev. B **45** 6435 (1992).
[4] M. B. Robin and P. Day: *Advances in Inorganic Chemistry and Radiochemistry*, ed. H. J. Emeleus (Academic, New York, 1967), Vol. 10, p. 217.
[5] P. Day: *Low Dimensional Cooperative Phenomena*, ed. H. J. Keller (Plenum, New York, 1974), p.191.
[6] H. J. Keller: *Extended Linear Chain Compounds*, ed. J. S. Miller (Plenum, New York, 1982), p. 357.
[7] H. Toftlund and O. Simonsen: Inorg. Chem. **23** (1984) 4261.
[8] K. Toriumi, Y. Wada, T. Mitani, S. Bandow, M. Yamashita and Y. Fujii: J. Am. Chem. Soc. **111** (1989) 2341.
[9] H. Okamoto, Y. Shimada, Y. Oka, A. Chainani, T. Takahashi, H. Kitagawa, T. Mitani, K. Toriumi, K. Inoue, T. Manabe and M. Yamashita: Phys. Rev. B **54** (1996) 8438.
[10] H. Okamoto, T. Mitani, K. Toriumi and M. Yamashita: Mater. Sci. Eng. B **13** (1992) L9.
[11] H. Shirakawa, T. Ito and S. Ikeda: Macromol. Chem. **179** (1978) 1565.
[12] I. B. Goldberg, H. R. Crowe, P. R. Newman, A. J. Heeger and A. G. MacDiarmid: J. Chem. Phys. **70** (1979) 1132.
[13] C. R. Fincher, Jr., M. Ozaki, A. J. Heeger and A. G. MacDiarmid: Phys. Rev. B **19** (1979) 4140.
[14] W. P. Su, J. R. Schrieffer and A. J. Heeger: Phys. Rev. Lett. **42** (1979) 1698.
[15] W. P. Su, J. R. Schrieffer and A. J. Heeger: Phys. Rev. B **22** (1980) 2099.
[16] H. Takayama, Y. R. Lin-Liu and K. Maki: Phys. Rev. B **21** (1980) 2388.
[17] S. Ichinose: Solid State Commun. **50** (1984) 137.
[18] Y. Onodera: J. Phys. Soc. Jpn. **56** (1987) 250.

[19] N. Kuroda, M. Sakai, Y. Nishina, M. Tanaka and S. Kurita: Phys. Rev. Lett. **58** (1987) 2122.
[20] H. Okamoto, T. Mitani, K. Toriumi and M. Yamashita: Phys. Rev. Lett. **69** (1992) 2248.
[21] C. Bellitto, A. Flamini, L. Gastaldi and L. Scaramuzza: Inorg. Chem. **22** (1983) 444.
[22] C. Bellitto, G. Dessy and V. Fares: Inorg. Chem. **24** (1985) 2815.
[23] C.-M. Che, F. H. Herbstein, W. P. Schaefer, R. E. Marsh and H. B. Gray: J. Am. Chem. Soc. **105** (1983) 4604.
[24] R. J. H. Clark, M. Kurmoo, H. M. Dawes and M. B. Hursthouse: Inorg. Chem. **25** (1986) 409.
[25] H. Kitagawa, N. Onodera, T. Sonoyama, M. Yamamoto, T. Fukawa, T. Mitani, M. Seto and Y. Maeda: J. Am. Chem. Soc. **121** (1999) 10068.
[26] S. Yamamoto: J. Phys. Soc. Jpn. **70** (2001) 1198.
[27] M. Kurmoo and R. J. H. Clark: Inorg. Chem. **24** (1985) 4420.
[28] L. G. Butler, M. H. Zietlow, C.-M. Che, W. P. Schaefer, S. Sridhar, P. J. Grunthaner, B. I. Swanson, R. J. H. Clark and H. B. Gray: J. Am. Chem. Soc. **110** (1988) 1155.
[29] N. Kimura, H. Ohki, R. Ikeda and M. Yamashita: Chem. Phys. Lett. **220** (1994) 40.
[30] Y. Wada, T. Furuta, M. Yamashita and K. Toriumi: Synth. Met. **70** (1995) 1195.
[31] M. Yamashita, S. Miya, T. Kawashima, T. Manabe, T. Sonoyama, H. Kitagawa, T. Mitani, H. Okamoto and R. Ikeda: J. Am. Chem. Soc. **121** (1999) 2321.
[32] B. I. Swanson, M. A. Stroud, S. D. Conradson and M. H. Zietlow: Solid State Commun. **65** (1988) 1405.
[33] M. A. Stroud, H. G. Drickamer, M. H. Zietlow, H. B. Gray and B. I. Swanson: J. Am. Chem. Soc. **111** (1989) 66.
[34] J. T. Gammel and G. S. Kanner: Synth. Met. **70** (1995) 1191.
[35] D. Baeriswyl and A. R. Bishop: Phys. Scr. **T19** (1987) 239.
[36] D. Baeriswyl and A. R. Bishop: J. Phys. C **21** (1988) 339.
[37] S. Yamamoto: to be published in Phys. Rev. B **64**, No. 10 (2001).
[38] H. Matsuzaki, H. Kishida, H. Okamoto, T. Kawashima, K. Takizawa, T. Ishii, H. Matsuzaka and M. Yamashita: unpublished.
[39] M. Kuwabara and K. Yonemists: to be published in J. Mater. Chem. **11** (2001).
[40] S. Yamamoto: Phys. Rev. B **63** (2001) 125124.
[41] S. Kivelson, T.-K. Lee, Y. R. Lin-Liu, I. Peschel and L. Yu: Phys. Rev. B **25** (1982) 4173.
[42] D. K. Campbell, A. R. Bishop and K. Fesser: Phys. Rev. B **26** (1982) 6862.
[43] Y. Onodera and S. Okuno: J. Phys. Soc. Jpn. **52** (1983) 2478.
[44] M. Nakahara: Phys. Lett. A **236** (1997) 97.
[45] S. D. Conradson, M. A. Stroud, M. H. Zietlow, B. I. Swanson, D. Baeriswyl and A. R. Bishop: Solid State Commun. **65** (1988) 723.
[46] J. T. Gammel, R. J. Donohoe, A. R. Bishop and B. I. Swanson: Phys. Rev. B **42** (1990) 10556.
[47] A. Mishima and K. Nasu: Phys. Rev. B **39** (1989) 5758.
[48] A. Mishima and K. Nasu: Phys. Rev. B **39** (1989) 5763.
[49] M. Suzuki and K. Nasu: Phys. Rev. B **45** (1992) 1605.
[50] K. Iwano and K. Nasu: J. Phys. Soc. Jpn. **61** (1992) 1380.
[51] Y. Tagawa and N. Suzuki: J. Phys. Soc. Jpn. **59** (1990) 4074.
[52] Y. Tagawa and N. Suzuki: J. Phys. Soc. Jpn. **64** (1990) 2212.
[53] S. Kurita, M. Haruki and K. Miyagawa: J. Phys. Soc. Jpn. **57** (1988) 1789.
[54] M. Haruki and S. Kurita: Phys. Rev. B **39** (1989) 5706.
[55] R. J. Donohoe, S. A. Ekberg, C. D. Tait and B. I. Swanson: Solid State Commun. **71** (1989) 49.
[56] K. Sakai, Y. Tanaka, Y. Tsuchiya, K. Hirata, T. Tsubomura, S. Iijima and A. Bhattacharjee: J. Am. Chem. Soc. **120** (1998) 8366.

TABLE I. Two estimates of the soliton width and mass fitting $Na_4[Pt_2(pop)_4I]\cdot 7H_2O$ of $E_g = 1.2\,\mathrm{eV}$ and $a = 8.9\,\text{Å}$, where we assume the BB and TS parametrizations (see text).

	BB parameters		TS parameters	
	ξ_s/a	M_s/m_e	ξ_s/a	M_s/m_e
S^-	1.2	94	2.4	28
S^+	0.7	160	1.6	42
S^0	1.1	100	2.1	31

TABLE II. Two estimates of the soliton width and mass fitting $Pt_2(dta)_4I$ of $E_g = 0.3\,\mathrm{eV}$ and $a = 8.6\,\text{Å}$, where we assume $t_{MM} = 2.0\,\mathrm{eV}$ and $t_{MM} = 1.5\,\mathrm{eV}$.

	$t_{MM} = 2.0\,\mathrm{eV}$		$t_{MM} = 1.5\,\mathrm{eV}$	
	ξ_s/a	M_s/m_e	ξ_s/a	M_s/m_e
S^-	6.2	12	4.7	19
S^+	6.0	12	4.5	20
S^0	6.1	12	4.6	19